Phase Difference Enhanced Imaging

Tetsuya Yoneda, Tomoyo Ideta, and Yasuhiro Hiai
School of Health Sciences, Kumamoto University, Kumamoto 862-0976, Japan

The phase image of MRI has a much high diagnosis potential. Susceptibility or another properties of tissue directly or indirectly affect on phase differences in the phase image. Therefore, it is possible to enhance a tissue's physical properties via phase differences. These enhanced images are great of use for discriminating the different tissues and further clinical applications.

In this paper, we report on new imaging technique "PhAse DiffRence Enhanced imaging (PADRE)" as an application of using the phase information in which we use a phase difference between tissues. This new technique can enhance the phase difference on the magnitude image, which corresponds to the local magnetic field difference caused by susceptibility difference, physical dynamics and so on. For comprehensive understanding of PADRE, a simple model is to be examined.

The enhanced tissue makes a higher contrast between different tissues, which is going to support the diagnosis of problems. We examine an improvement of contrast by using the PADRE thorough a comparison between a CNR of experimental data and theory which we introduced.

Discussions and results of this paper determine the best imaging parameters. We can see wonderful appearance of small vessels in the brain by using these parameters.

Key Words; MRI, Phase image, Enhancement of Phase difference, PRESTO, Susceptibility

I. INTRODUCTION

Magnetic Resonance Imaging (MRI) is one of the powerful tools in clinical site. In these decades, many sequences have been developed[1] in order to make an accurate diagnosis which demands much information of tissues. T_1 and T_2 weighted imagings, for example, are very famous sequences for making a discrimination of tissues in the body. Especially, wealth of sequences is applied for diagnosis of many kinds of disorder in the brain.

To date, almost all sequences have been designed for create magnitude image. Needless to say, magnitude image is a vital portion of the MRI-image and diagnosis tool. The signal of magnitude image represents "magnitude" of complex signals which show hydrogen spin density in the body directly or indirectly[2),3)]. The hydrogen spin density" is very meaningful information of the body. This is because hydrogen atoms are mainly contained in the water molecule which is the principal abundance in the human body[4)]. Consequently, all tissues contain water molecule insomuch that the disorder like a tumor also contains it. Therefore, to catch signal from the disorder tissues, the hydrogen atom is thought of as very important for diagnosis and also magnitude image is.

The signal of image is made up of real and imaginary numbers i.e. complex numbers. Similarly, complex image can be divided into magnitude image and other half "phase image". Signal of phase image represents phase of complex signal which also plays an important role to construct magnitude image. Since the signal in a one pixel is reconstructed by averaged signals in the pixel, signals in the region of pixel which have random phases produce no signal intensity as a pixel value. This is also the case in k-space, therefore, we need a uniform phase signals to reconstruct magnitude image and also phase image. Additionally, phase signal contains much information of tissues. For instance, magnetism of tissues strongly affects on phase values. By extracting information such the phase differences from phase values, we can sometimes find certain serious problems in the human body.

Recently, phase information has greatly attracted attentions[5)-7)]. Lots of studies are shown and we can find excellent successes and progresses therein[8)-12)]. Techniques, treatments and developments using phase information now become a central object of interest in the world. Many researchers think that phase information is to be a subsidiary but great tool to aid diagnosis.

In this paper, we propose a technique using phase information and analyze images which are produced by our technique. This technique uses "*phase difference*" of phase images and enhances them on corresponding magnitude images, which is called PhAse DiffeRence Enhanced imaging (PADRE).

We are going to show the outline of theory of PADRE in section II in which we also introduce a simple electromagnetic model for comprehensive understanding what is a key to produce phase difference in the human body. In section III, detailed conditions for taking images and tools for analysis of PADRE-images are suggested. Results and discussions are presented in section IV and V, respectively. Conclusions are also shown in section V.

II. THEORY

First of all, we have to touch the outline of our PADRE theory. As is well known, the complex signals $S(k) = |S(k)|e^{-i\theta(k)}$ at general point k in the k-space are transformed into complex image signal $\rho(x) = |\rho(x)|e^{i\phi(x)}$ at a point x in the image space by the Fourier Transformation, where θ and $\phi(x)$ is a phase at k and x respectively. Note that, thorough this paper, scalar representation of

coordinate like x, k means general coordinate (vector representation) i.e. x contains x and y coordinates simultaneously. We sometime show a individual points by using subscript; x_i, etc.

Phase value is proportional to echo time (TE) and the magnetic field $B(x)$ (in this paper, we call the magnetic flux density as the magnetic field), which can be represented by $-\gamma B(x)$TE where γ is the gyromagnetic ratio. Therefore, if we use long TE, the phase has the large positive or negative value and can not be shown in the phase image because of an upper and lower limits of pixel value. This limitations cause "*phase wrapping*" which shows the 2π symmetry of phase $\phi(x)$[10),13),14)]. Unfortunately, this phase wrapping plays tricks on a PADRE-image as a result of phase difference enhancing.

In the last decade, many kinds of unwrapping method are suggested in order to remove the phase wrapping difficulties in the wide area of study. We can roughly classify them into two kinds. First, unwrap the restricted phase into all range,

$$\phi(x) \longrightarrow \phi'(x), \tag{1}$$

where $\phi(x)$ has the range $-\pi < \phi(x) \leq \pi \pmod{2\pi}$, while $\phi'(x)$ has an arbitrary range. This unwrapping method produces a true value of phase, so that sometimes gives a different phase value even for tissues which are same kind but locate in different points in the image. Such a large difference of phase for same kind tissues which may or may not show as a different tissues on an image is not always useful from the diagnostic point of view. The second is rather useful. In this method, $\phi'(x)$ looks having the same range, that is $-\pi < \phi'(x) \leq \pi$, but no 2π symmetry exists. The meaning of this restriction is very important for clinical applications and can be understood thorough the following discussion.

Phase wrapping is frequently seen near boundary between the air and tissue. At such the boundary, large magnetic field difference $\Delta B(x)$ is induced due to a large difference of susceptibility between them. As is mentioned, therefore, long TE leads a large phase difference $\Delta\phi(x)$ with large $\Delta B(x)$. This reads

$$\begin{aligned} \Delta\phi(x_0) &= -\gamma \Delta B(x_0)\mathrm{TE}, \\ \Delta B(x_0) &\equiv B_1(x_0,\chi_1) - B_2(x_0,\chi_2), \\ B_i(x_0,\chi_i) &\equiv \lim_{x\to x_0} B_i(x,\chi_i), \quad (i=1,2), \end{aligned} \tag{2}$$

where $B_1(x_0,\chi_1)$ and $B_2(x_0,\chi_2)$ is the magnetic field with susceptibility χ_1 and χ_2 respectively at the boundary x_0. In other words, large phase differences are induced by large susceptibility differences between different tissues. We can find an effect of susceptibility difference at a boundary between an air in the body and surrounding tissue as an artifact. In a brain image, the frontal sinus induces a large susceptibility difference at the boundary of brain. One can find many "*streaks*" because of phase wrapping in the phase image around frontal part of brain. These streaks annoy us to create a clear image in the long TE. As is easily seen from Eq.(2), however, we need to use the long TE to obtain the enough phase difference. Hence, we always face on the phase wrapping problem when we want to use the information of phase difference.

Fortunately, the streaks induced by phase wrapping almost always have the large period compared with the size of tissue structures. By applying the filter on k-space, we can remove the large periodic streaks in the both of images of magnitude and phase. We adopt the mathematical procedure of filtering in order to remove the phase wrapping described as follows.

The complex signal $S(k)$ is filtered by low-pass filter $L(k)$ in order to create the only low-frequency components contained image. A filtered signal $S'(k)$ is

$$S'(k) = L(k)S(k), \tag{3}$$

so that the filtered image $\rho'(x)$ is to be

$$\rho'(x) = |\rho'(x)|e^{i\phi'(x)} \equiv \int_{-\infty}^{\infty} S'(k)e^{-ikx}dk. \tag{4}$$

This integration is nothing but convolution of $\mathcal{F}[L]$ and $\mathcal{F}[S]$, where $\mathcal{F}[L]$ and $\mathcal{F}[S]$ is Fourier Transform of $L(k)$ and $S(k)$, respectively. A complex division of image signal by $\rho'(x)$ produces an high-pass filtered phase $\phi''(x)$ which contains only high frequency components, namely tissue's phase difference information.

$$\rho''(x) = |\rho''(x)|e^{i\phi''(x)} \equiv \frac{\rho(x)}{\rho'(x)}. \tag{5}$$

In general, this high-pass filtered phase and magnitude image are created by averaging a data by neighbor data which are at $x \pm \Delta x$, where $\Delta x \sim 1/\text{Filter size}$. In that sense, a value of high-pass filtered phase image simply shows a phase difference $\Delta\phi(x)$ which should correspond to Eq.(2) and have no phase wrapping any more.

It is worth pointing out here that this equivalent high-pass filtering technique dose not induce any artifacts related to filtering because of complex division which just affects on phase component.

The phase differences are deeply related to a tissue differences connecting to its magnetic properties. For example, arterial and venous blood have the slightly different magnetic properties each other. These properties come from differences of the fractional oxygenation of red cell in the blood. Since oxyhemoglobin is a diamagnetic material and deoxyhemoglobin is a paramagnetic material, magnetic field difference arises around a deoxyhemoglobin but less difference around an oxyhemoglobin because the human body averagely has a diamagnetic property. Therefore, many spin decoherences (signal decreases) are induced in/around the venous vessels than in/around the arterial vessels and another tissues, which is well known as the blood oxygenation level dependent (BOLD) effect[1),15)−17)] . This effect is one of the useful causes to create large phase difference on the phase

image. Adopting BOLD effect in order to make clear tissue discriminations, it means that a susceptibility differences are indirectly enhanced thorough the phase differences. Note that intravascular phase difference induced by BOLD effect contains a flow effect[18]. In this sense, discrimination using phase difference is not exactly same meaning of susceptibility weighted imaging (SWI)[5]. In this paper, we simply use the phase difference without flow compensation or another technique to extract susceptibility difference, i.e. PADRE is not same as SWI.

One of the important applications of PADRE with BOLD effect is making strong contrasts between vessels and tissues as a background, especially in the brain. Up to here, we did not touch about the mathematical methods to reflect the phase differences onto image.

Suppose that we have already had the phase difference information $\Delta\phi(x)$, and known the enhancing function $w(x, \Delta\phi)$ of a position x which is designed for making phase difference on magnitude image strongly. All we have to do is to multiply the enhancing function on the original magnitude image $|\rho(x)|$. An enhanced image $|\rho_f(x)|$ reads

$$|\rho_f(x)| \equiv w(x, \Delta\phi(x))|\rho(x)|. \tag{6}$$

The PADRE-image is finally obtained by this enhanced signal $|\rho_f(x)|$. In this image, signals of enhanced parts are decreased by applying w, therefore it can happen that a size of objective tissue becomes larger than the true size which is caused by leakage of magnetism from the objective tissue. One may see such an effect on the vessels because of rather strong magnetism of hemoglobin as is described.

To get comprehensive understanding of the role of above enhancing function and leakage mechanism of magnetism from vessels, a cylinder which has the infinite length is very useful as a simple model of vessel[1),18),19)]. Let the cylinder have a radius a and susceptibility χ inside the cylinder. If direction of static magnetic field B_0 is perpendicular to the cylinder axis (z-axis) and is along the x-axis, we have

$$\Delta B(x) = \begin{cases} -\dfrac{\Delta\chi}{6} B_0 & :\text{Internal}, \\ \dfrac{(\Delta\chi)a^2}{2r^2} \cos 2\theta B_0 & :\text{External}, \end{cases} \tag{7}$$

where r is a distance from the center of cylinder to an external point , θ is an angle from the static magnetic field and $\Delta\chi$ is a susceptibility difference between internal material and external material (Fig.1). For the maximal simplicity, we assume that the susceptibility of external cylinder is zero, so that susceptibility of the internal cylinder is automatically equivalent to susceptibility difference $\Delta\chi$.

This model shows that if $\Delta\chi > 0$, by plugging Eq.(7) into Eq.(2), the phase difference of internal cylinder is to be always negative. The induced phase difference of external cylinder, however, shows much complicated behavior (Fig.2). A positive phase difference is induced in the direction of static magnetic field, while a negative one is also induced in the direction perpendicular to the static magnetic field on the same plane. This result tells us that if we apply the enhancing function to the both of signs, the area of cylinder in which signals should be seen low intensity becomes larger than the original one due to the enhancing function's depression of signals. In Fig.3 which corresponds to Fig.2 we set $w(x, \Delta\phi) = (1 - |\Delta\phi|/\pi)$, $\Delta\phi < 0$, i.e. linearly weighted to the negative phase difference, while we put unity for $\Delta\phi \geq 0$[1),5)]. Note that the sign of phase differences are changed by Eq.(2) in the same direction in Figs.2 and 3. For the positive phase difference, we set w unity which means no depression happens. As a result of this discussion on simple cylinder model of vessel, one may easily understand the change of size of objective tissue in a PADRE-image. This result also tells us that if we adopt the negative phase difference for enhancing phase difference, the size of vessel does not change in the direction perpendicular to the B_0. These effect can be observed in Fig.4.

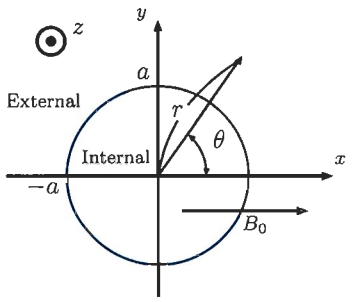

FIG. 1: Radius of cylinder is a. A point in external cylinder x locates at $r = |x|$ from origin with angle θ.

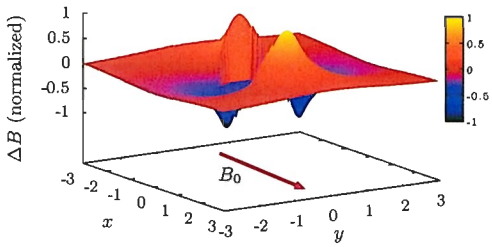

FIG. 2: The behavior of normalized magnetic field difference $\Delta\phi(x)$. Both of positive and negative field difference can be seen.

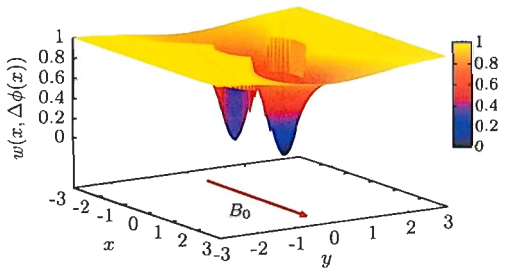

FIG. 3: An enhancing function $w(x, \phi(x))$ is plotted. This function does not enhance the positive phase difference.

In T_2^* weighted imaging, the size of vessel sometimes becomes larger than the original one. This phenomenon resembles that of PADRE, but does not root on the same reason. The depression of signal in T_2^* imaging is simple reflection of the T_2^* relaxation which is caused by many reasons (interaction among the molecules and atoms, partial phase transition of materials, changing the magnetisms and so on). The leakage of magnetism and strong magnetism are candidates generating T_2^* relaxation. The PADRE-image, of course, contains the T_2^* relaxation effect due to the long TE, but does not always have the same depressed area which depends on sort of enhancing function in PADRE: In the cylinder model, T_2^* imaging feels and shows the T_2^* nonuniformity in both of directions, while enhancing direction in PADRE can be chosen. In other words, phase difference mainly caused by susceptibility difference induces T_2^* nonuniformity, but the reverse is not always the case. Therefore, we can conclude that there are not one to one correspondences between PADRE and T_2^* imaging.

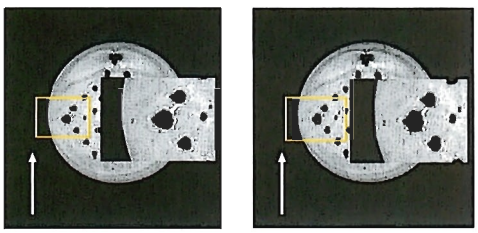

FIG. 4: Images of phantom study. The direction of the magnetic field is represented by white arrow. In PRESTO-image (a), signal around the tube is depressed both of directions parallel to and perpendicular to the magnetic field B_0 due to the T_2^* relaxation. In PADRE-image (b), signal of external tube is depressed much more only along the direction parallel to the magnetic field.

III. MATERIALS AND METHODS

3D-gradient echo images were acquired on the 3T system (Achieva 3.0, Philips, Netherlands) with PRESTO sequence. Sequence parameters were as follows; TE = 52 ms, TR = 32 ms, FA = 10°, FOV = 230×230 mm^2, slice thickness = 2 mm (100 slices with spacing between slices = 1mm), acquisition matrix = 512×489 (reconstructed in 512×512) and acquisition time was about 15 minutes. The magnitude and phase data were obtained as DICOM data, and PADRE-images are generated by program using C language. One healthy volunteer (46 years old, male) images were taken with informed consent.

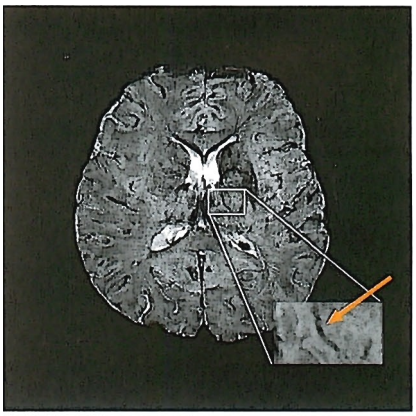

FIG. 5: We measure magnitude image produced by PRESTO sequence. We selected thalamus as background for the vessel (arrow).

FIG. 6: Phase image corresponding to Fig.5. One can see a streaks of phase wrapping. These streaks are induced by large magnetic differences on the edge of head.

Very small vessels can be seen on the magnitude image shown in Fig.5, and the wrapping streaks on the phase image are appeared due to the long TE (Fig.6), which should be removed for creating the phase differences. We had selected a common Region Of Interest (ROI) for magnitude and phase image which satisfies a condition; parenchyma have a uniform signal i.e. difference between a value of signal in ROI and averaged value of signals is sufficiently small. This condition looks tightly bounded one. Although, we need to use such the condition for making the analysis of data clear and simple. We will touch the reason to use of this condition soon.

The window size of high-pass filter were selected 32×32, 64×64, 128×128, 256×256 and Hamming filter was used as filter function for the simplicity. In this paper, we call the filter size of low-pass filter in k-space as the window size of high-pass filter. The enhancing function was chosen

$$w(x, \Delta\phi(x)) \equiv \left(1 - \frac{|\Delta\phi(x)|}{\pi}\right)^m, \quad \text{for } -\pi < \Delta\phi(x) \leq \pi, \tag{8}$$

where m is real positive number which we call multiplying number. As is easily seen, for $m > 1$, w does not enhance the phase differences linearly. In this paper, we had studied using integers $m = 2, 3, 4, 5, 6$ and 7 for also the simplicity. Note that, in PADRE, we did not restrict to m being positive integer. We can essentially use any real number for m and also any kind of enhancing function w.

Complex images generated by combining the magnitude with phase images are Fourier Transformed into complex k-space data. By applying the high-pass filter on the k-space data, PADRE-images and phase difference images were obtained.

We had chosen a vessel to measure (arrow) and ROI of the signal as the background in the thalamus because of uniformity of signal. The number of pixel of ROI is 80 pixels[20] and fixed thorough the study. Mean value is used as a background signal on PADRE-image and phase difference image. Standard Deviation (SD) on the image was collected in the ROI. We assume that SD of signal which is noise on the image has a same value denoted by σ on the both of vessel signal area and phase difference signal area in the same image.

Contrast Noise Ratio (CNR) are derived from the collected data. Theoretical prediction of CNR of this study is also calculated and plotted. Let $|\rho_{f1}(x_1)|$ and $|\rho_{f2}|$ is signal of vessel and background respectively. Note that the signal of background has only phase coordinate because information of position of data is suppressed by averaging over ROI, and we sometimes do not explicitly show the variables x and $\Delta\phi$ in an expressions of functions.

$$|\rho_f| \equiv w(\Delta\phi)\overline{|\rho|}, \tag{9}$$

$$\Delta\phi \equiv \frac{1}{\text{number of pixel}} \sum_{\ell}^{\text{number of pixel}} \Delta\phi(x_\ell),$$

$$\overline{|\rho|} \equiv \frac{1}{\text{number of pixel}} \sum_{\ell}^{\text{number of pixel}} \rho(x_\ell).$$

From Eq.(A.3), we have theoretical CNR

$$\text{CNR} \simeq \frac{1}{\sigma} \frac{||\rho_{f1}(x_1, \Delta\phi_1)| - |\rho_{f2}||}{\sqrt{\sum_{j=1,2} \hat{\mathcal{L}}(\Delta\phi_j) w(x_j, \Delta\phi_j)}}, \tag{10}$$

$$\hat{\mathcal{L}}(\Delta\phi_j) \equiv \left(\frac{\partial}{\partial\Delta\phi_j}\right)^2 + 1,$$

where ϕ_1 and ϕ_2 represents a phase difference in vessel and mean value of phase difference of background, respectively. To drive Eq.(10), the signal and phase difference of background is averaged over ROI and is assumed that each values of signal $|\rho_f(x_i, \Delta\phi_i)|$ in ROI does not differ from averaged value $|\rho_f|$ which means

$$\begin{aligned} &||\rho_f(x_i, \Delta\phi)| - |\rho_f|| \\ &\quad \leq |\rho(x_i)| \cdot |w(x_i, \Delta\phi(x_i)) - w(\Delta\phi)| \\ &\qquad + |w(\Delta\phi)| \cdot ||\rho(x_i)| - \overline{|\rho|}| \ll 1, \\ &\qquad\qquad x_i \in \text{ROI} \end{aligned} \tag{11}$$

with a help of Eq.(6) and Eq.(9). In order to satisfy the above inequality, we need uniform background signal of magnitude and phase.

IV. RESULTS

PADRE-images are strongly affected by both of the window size and the multiplying number in the enhancing function. For example, in Fig.7, we can find the many streaks (artifacts) in the image with small window size, while streaks can be removed with large window size. This is the very effect of high-pass filter. In Fig.8, contrast of images look likes to increase as multiplying number increases.

CNR of these images are plotted in Fig.9. Curves with $m = 4, 5$ have a high CNR in window size > 100. For m =2, 3, 6, and 7, CNR are lower compared with magnitude image.

The theoretical curve is also plotted with experimental data in Fig.10. We can see the theoretical curve (surface) can fit the experimental curves, especially, very nice fitting can be seen for m =2 and 3. The theoretical curve is simulated by Eq.(10) which does not contain the change of the window size, so that it depends only on the multiplying number. This is one of the reason why the theoretical curve looks linearly increase by change the multiplying number and does not fit along the window size.

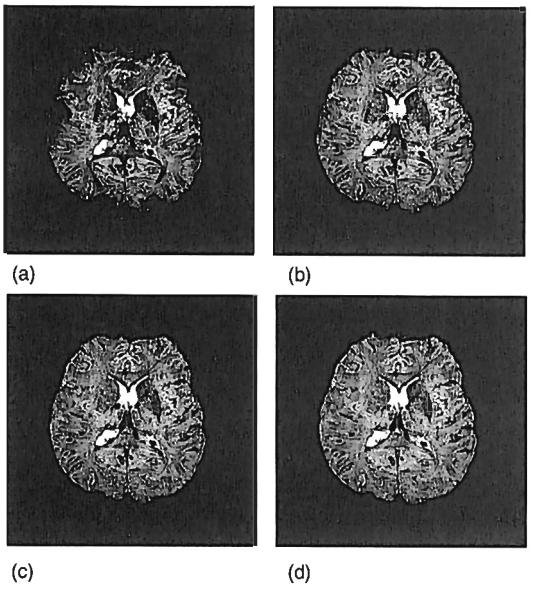

FIG. 7: PADRE-images with changing the window size; (a) $W = 32$ (b) $W = 64$ (c) $W = 128$ (d) $W = 256$. Artifact are reduced by increasing the window size.

V. DISCUSSIONS AND CONCLUSIONS

Fig.10 tells that theoretical CNR becomes higher by increasing the window size and multiplying number. However experimental results in Fig.9 shows higher CNR in larger window size and maximum point at $m = 5$. This is, at a glance, a contradiction in the prediction of theory.

Such a contradictory behavior of theoretical curve is to be understood thorough a reconsideration of assumption of uniformity of SD. When we calculate theoretical curve in this paper, we had assumed that SD of every tissue has same value σ which is independent of on x and $\Delta\phi$. But this assumption is not always true in the experimental results. As is seen in Fig.11 and 12, σ slightly depends on the window size and number of multiplying. Therefore, we need take these dependences into account for analysis of CNR.

We can explain the behavior of CNR by using the noise and phase dependences against the multiplying number and the window size. SD of background, from Fig.11, is gradually and linearly decreased with the window size value W for a fixed m, which can be represented by $-a(W-b)$ with positive constants a and b ($W < b$ is reasonably assumed in the used range shown in Fig.11). It can be assumed by Fig.11 that both of phase differences have an extremum at or around $W = 128$ and behave as a quadratical function.[22] In such case, a question – "can we realize the monotonically increasing behavior of

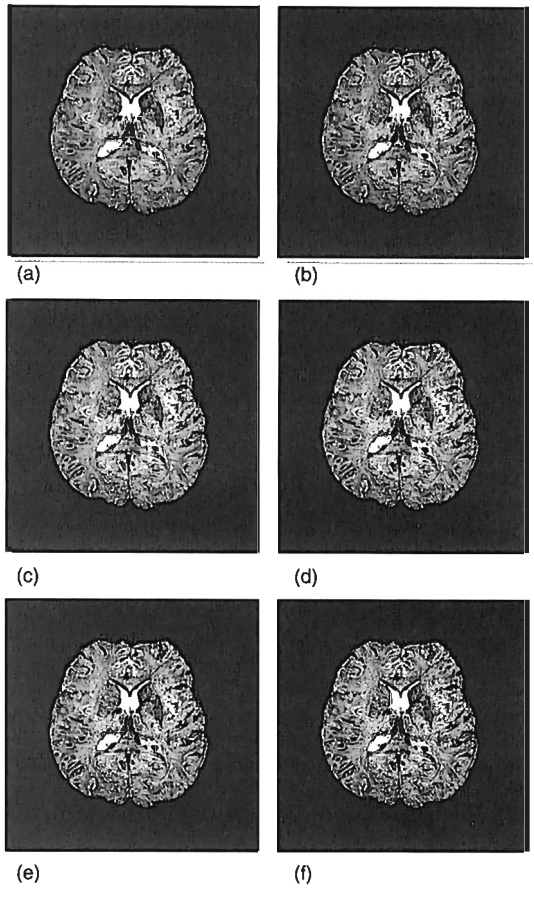

FIG. 8: PADRE-images with increasing multiplying number; (a) $m = 2$ (b) $m = 3$ (c) $m = 4$ (d) $m = 5$ (e) $m = 6$ (f) $m = 7$. The larger multiplying number becomes, it looks, the better contrast becomes.

CNR shown in Fig.9 under above phase behavior?" – naturally arises. To resolve this question, we should check that CNR increases as is in Fig.9 even at the extremum point, otherwise, by strongest enhancement at the extremum point, we would still have a suspicion that CNR being to have "*a maximal value*" at the extremum point of phase.

Let extremum point which we mentioned be W_0, derivatives of the enhancing function become

$$\left.\frac{\partial w(W)}{\partial W}\right|_{W=W_0} = 0, \quad \left.\frac{\partial^2 w(W)}{\partial W^2}\right|_{W=W_0} > 0. \qquad (12)$$

The second inequality is come from the fact that $w(W_0)$ should has a extremal minimum value. We use a simple notations like $w(W)$ to apparently show a variable what we are now concentrating (as is already commented, some

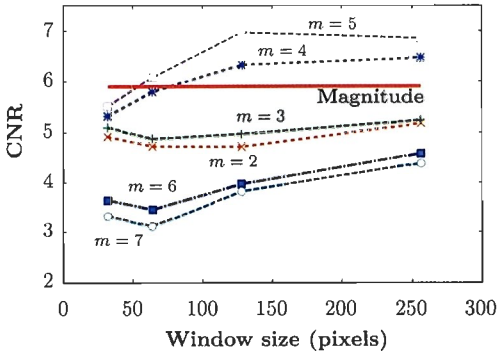

FIG. 9: CNR curves. The solid red line "Magnitude" represents CNR of vessel in original magnitude image. A combinations of multiplying numbers $m = 4$ or $m = 5$ and window size of filter 128 or 256 are recommended to make a PADRE-image.

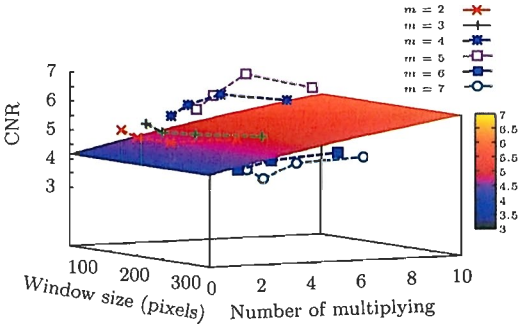

FIG. 10: CNR curves derived from PADRE images vs. theoretical surface (curve) which we derived using average vales of phase of a vessel and a tissue. The theoretical curve is fitted well, especially in lower m.

of variables are omitted for simplicity). In this case, CNR and its derivative with fixed m are approximately represented

$$\mathrm{CNR}(W) \simeq \frac{Aw_1(W) - Bw_2(W)}{-a(W-b)}, \quad (13)$$

$$\frac{\partial \mathrm{CNR}(W)}{\partial W} \simeq \frac{Aw_1'(W) - Bw_2'(W)}{-a(W-b)} + \frac{Aw_1(W) - Bw_2(W)}{a(W-b)^2} > 0. \quad (14)$$

The prime in above equation represents partial derivative with respect to W and w_i shows i-th tissue's enhancing function with magnitude image denoted by A and B. In this case, first and second term in numerator of CNR

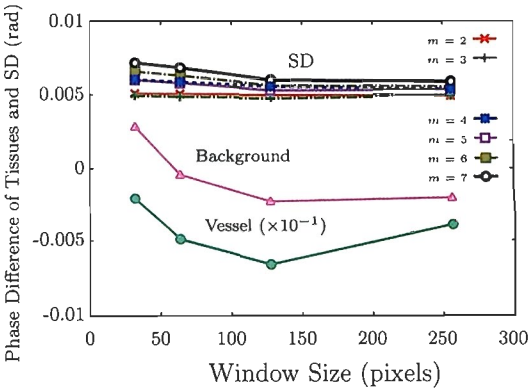

FIG. 11: Behavior of phase difference and SD in radian. Lines of SD look being inclined to be decrease linearly or being constant, while phase difference of background and vessel behave a quadratical function of the window size.

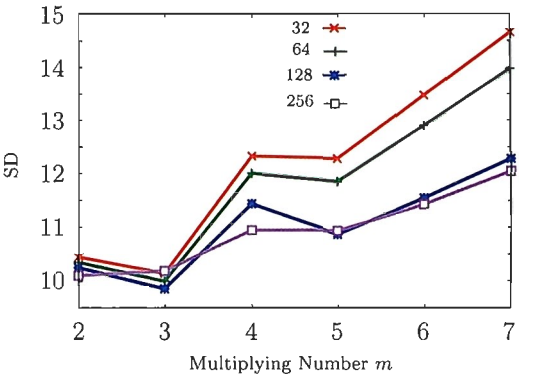

FIG. 12: Behavior of SD are plotted in multiplying number. All of them have a form of linear function or quadratical function of multiplying number.

is PADRE signal of back ground and vessel respectively. From Fig.11, numerator of CNR and its derivative are always positive because of significant order difference between phase of back ground and vessel. Finally, we can have Eq.(14) which means monotonically increasing of CNR.

By plugging Eq.(12) into Eq.(14), we can also check behavior of CNR at W_0.

$$\frac{\partial}{\partial W}\mathrm{CNR}(W)\Big|_{W=W_0} \simeq \frac{Aw_1(W) - Bw_2(W)}{a(W_0-b)^2}\Big|_{W=W_0} > 0. \quad (15)$$

In the similar way, we can derive that second derivative of CNR is positive at W_0,

$$\frac{\partial^2}{\partial W^2}\mathrm{CNR}(W)\Big|_{W=W_0} > 0. \qquad (16)$$

Therefore, CNR increases monotonically in W, even for the case when w being at an extremum point W_0.[23)]

For fixed W, phase differences are fixed and SD are quadratically increasing in accordance with increasing of m. As the result of these parameter's behaviors, CNR should increase for a larger m because phase difference becomes much faster than increasing of SD according to Eq.(9). This had been already shown by theoretical calculation shown in Fig.10. As is already touched, theoretical curve can not predict experimental curves correctly. From the theoretical point of view, we need modify the derivation of Eq.(10) by taking a behavior of the window size and the multiplying number into account. This is somewhat difficult derivation because of complicated entanglements among many parameters. We would like to set them further study.

In this discussion, we try to approach to this problem from rather easy way. One can plot the curves of contrast vs. number of multiplying Fig.13. According to

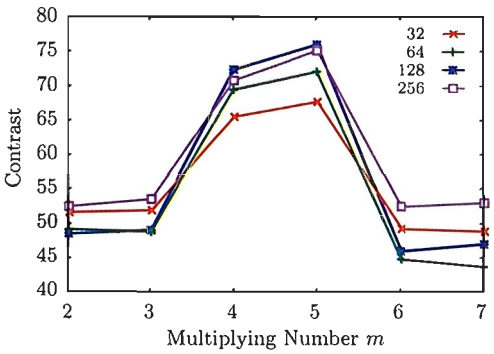

FIG. 13: Theoretically, contrasts with fixed window size should monotonically increase. But we can see the jump around m =5 to 6.

the theoretical calculation, contrast should become larger with increasing the multiplying number, on the contrary experimental contrasts do not increase. We can see the dramatic decreasing of contrast between m = 5 and 6. We consider this decreasing is caused by unexpected signal increasing of surrounding background by enhancing the positive and negative phase differences which are contained in background. The blood in vessel, especially in vein, almost always has somewhat large negative phase difference compared with that of background which fluctuates about mean value 0 with σ, so that phase difference of background "always" has the both of positive and negative value[24)]. Therefore, enhancing function can decrease an averaged signal value in PADRE-image, and as the result, suddenly depression of CNR is arisen.

FIG. 14: Minim Intensity Projection image of PRESTO-image on which 8 slices of PRESTO-images are projected. We can see the many small vessels in this image. This is due to long TE.

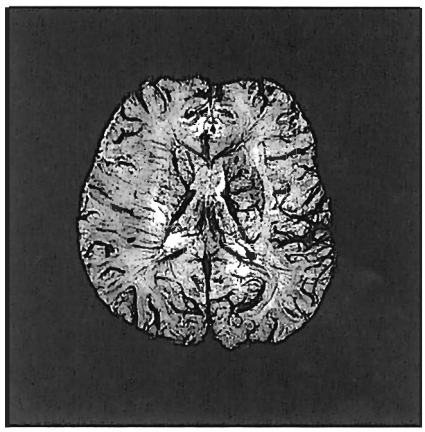

FIG. 15: Miniped image of PADRE-images projected over 8 slices with m = 5, W = 128. The contrast between vessels and background is clearly high and even small vessels are appeared.

We have to refer an advantages of PRESTO-sequence in PADRE. PRESTO originally has high enough vessel-tissue contrast as is seen in Fig.9. This is due to the long TE, and therefore strong T_2^* dephasing happens. Thanks to the long TE produced by PRESTO, we can see the large phase differences in PADRE. This affects on even smaller vessels in the image and make the contrast between surrounding tissues and smaller vessels. It can be

seen in the PADRE-images that such smaller vessels are appeared in minimum intensity projection (mIP, minip) images of PADRE-images. We can compare mIP image of PRESTO-image Fig.14 with mIP image of PADRE-image Fig.15. By comparison, contrast in PADRE-image between vessel and parenchyma clearly becomes much better than that in PRESTO-image. One of the another advantages of using PRESTO is reducing the acquiring time. This advantage is also very useful from the clinical point of view.

In this paper, we had investigated on new technique named PADRE in which we use phase information in order to mainly enhance the local magnetic field difference through the discussion of CNR. The enhancement had carried out for both of the phase difference signs. In such case, it was revealed that best multiplying number and window size was $m = 5$ and $W = 128$, respectively.

For further research, we need to develop an new CNR formula which contains the complicated relations among many parameters. We also have to introduce the TE (TR) dependence on the magnitude and phase images because of clinical demands.

Acknowledgments

Authors would like to thank Mr. T. Sakamoto for taking the images and showing us the many useful suggestions, and Professor S. Katsuragawa for carefully reading this paper.

APPENDIX

In this appendix, we derive the theoretical CNR in PADRE-image. We consider the case that a signal of objective tissue locating at x_1 and background locating at x_2 have signal value $|\rho_1(x_1)|$ and $|\rho_2(x_2)|$, and phase difference $\Delta\phi_1(x_1)$ and $\Delta\phi_2(x_2)$ respectively. Assume that background signal and phase difference are almost uniform in a ROI, and SD of objective tissue and background are same. Note that x_1 is the "point" but x_2 shows the general point of background i.e. ROI. Each elements of ROI is to be represented by $x_{2i} \in$ ROI.

We may replace

$$|\rho_{\mathrm{f}}(x_2)| \sim \overline{|\rho_{\mathrm{f}}|}, \tag{A.1}$$

by virtue of the assumption of uniformity in background. The definition of $\overline{|\rho_{\mathrm{f}}|}$ is given by Eq.(9). Hence, the contrast between signal and background becomes

$$\mathrm{Cont}(x_1) \equiv ||\rho_f(x_1, \Delta\phi_1)| - \overline{|\rho_{\mathrm{f}}|}|. \tag{A.2}$$

The derivation of total SD σ_{tot} for the contrast is something awkward. Propagation of uncertainly tells

$$\begin{aligned}\sigma_{\mathrm{tot}}^2 &\simeq \sum_{i=1,2}\left[\left(dx_i\frac{\partial}{\partial x_i}\right)^2 + \left(d\Delta\phi_i\frac{\partial}{\partial\Delta\phi_i}\right)^2\right]\mathrm{Cont}(x_1)\\ &= \sigma^2\sum_{i=1,2}\left[1+\left(\frac{\partial}{\partial\Delta\phi_i}\right)^2\right]w(x_i,\Delta\phi_i).\end{aligned} \tag{A.3}$$

In last equality, we used $d\Delta\phi_i = \sigma/|\rho(x_i)|$.

REFERENCES

1) Haacke E. M. et al.; Magnetic Resonance Imaging, John Wiley & Sons, New York, 1999.

2) Levitt, M. H.; Spin Dynamics, John Wiley & Sons, New York, 2001.

3) Slichter, C. P.; Principle of Magnetic Resonance, Springer-Verlag, Berlin, 1978.

4) Iwama T. et al.; Proton Nuclear Magnetic Resonance Studies on Water Structure in Peritumoral Edematous Brain Tissue. Magn Reson Imaging 24: 53-63, 1992.

5) Haacke E. M. et al.; Susceptibility Weighted Imaging (SWI). Magn Reson Med 52: 612-618, 2004.

6) Rauscher A. et al,; Nonnvasive Assessment of Vascular Architecture and Function during Modulated Blood Oxgenation Using Susceptibility Weighted Magnetic Resonance Imaging. Magn Reson Med 54: 87-95, 2005.

7) Sehgal V. et al.; Clinical Applications of Neuroimaging With Susceptibility-Weighted Imaging. J Magn Reson Imaging 22: 439-450, 2005.

8) Wang Y. et al.; Artery and Vein Separation Using Susceptibility Dependent Phase in Contrast-Enhanced MRA. J Magn Reson Imaging 12: 661-670, 2000.

9) Reichenbach J. R. et al.; High-Resolution MR Venography at 3.0 Tesla. J Comput Assist Tomogr 24(6): 949-957, 2000.

10) Rauscher A. et al.; Automated Unwrapping of MR Phase Images Applied to BOLD MR-Venography at 3 Tesla. J Magn Reson Imaging 18: 175-180, 2003.

11) Bourgeat P. et al.; MR image segmentation of the knee bone using phase information. Medical Image Analysis 11: 325-335, 2007.

12) Haacke E. M. et al.; Establishing a Baseline Phase Behavior in Magnetic Resonance Imaging to Determine Normal vs. Abnormal Iron Content in the Brain. J Magn Reson Imaging 26: 256-264, 2007.

13) Hedley M. et al.; A New Two-Dimensional Phase Unwrapping Algorithm for MRI Images. Magn Reson Med 24: 177-181, 1992.

14) Huntley J. M.; Three-Dimensional Noise-Immune Phase Unwrapping Algorithm. Appl Opt 40(23); 3901-3908, 2001.

15) Ogawa S. et al.; Brain Magnetic Resonance Imaging with Contrast Dependent on Blood Oxygenation. Proc Natl Acad Sci USA 87: 9868-9872, 1990.

16) Haacke E. M. et al.; 2D and 3D High Resolution Gradient Echo Functional Imaging of the Brain: Venous Contributions to Signal in Motor Cortex Studies. NMR in Biomedicine 7: 54-62, 1994.

17) Haacke E. M. et al.; In Vivo Measurement of Blood Oxygen Saturation Using Magnetic Resonance Imaging: A Direct Validation of the Blood Oxygen Level-Dependent Concept in Functional Brain Imaging. Human Brain Mapping 5: 341-346, 1997.

18) Haacke E. M. et al.; In Vivo Validation of the BOLD mechanism: A Review of Signal Changes in Gradient Echo Functional MRI in the Presence of Flow. Int J Imaging Sys Tech 6: 153-163, 1995.

19) Xu Y. et al.; The Role of Voxel Aspect Ration in Determining Apparent Vascular Phase Behavior in Susceptibility Weighted Imaging. Magn Reson Imaging 24: 155-160, 2006.

20) This pixel number of ROI is quite reasonable. This study had used PRESTO sequence which is parallel imaging, and therefore when we take the noise of background and vessel we need to pay spacial attention because the signal of outside of body in the image in which we ordinarily use a ROI for collecting the noise is automatically corrected as zero. According to the latest report[21], we must use the uniform tissue for taking the noise and size of ROI should be larger than 50 pixels and less than order of 100.

21) Ogura A. et al.; Method of SNR Determination Using Clinical Images. Jpn J Radiol Technol 63(9): 1009-1104, 2007. in Japanese.

22) One should note that significant order difference between SD and phase of a Vessel. The curves in Fig.11 have different function shapes due to this order difference. Therefore, behavior of SD should be different from one of phase of vessel. Dependence of phase of vessel is especially important because CNR mainly depends on phase of vessel through the enhance function due to order difference. Additionally, one should notice that another order difference, that is, between phase of back ground and vessel. This ensures positivity of CNR and its derivative.

23) It is sometimes misread that behavior of CNR is directly affected by one of phase difference which is pointed out in 22). In PADRE case, behavior of CNR depends on one of enhance function. It is true that "*behavior of signal* " is directly affected by its phase difference behavior but is "*not true*" for CNR because CNR is defined as difference between signals of two tissues with a noise. Therefore, we need to take both of two signals on PADRE into consideration carefully.

24) Some of blood in vessel "sometime" has the positive sign of phase difference. This is due to the rather strong paramagnetism of surrounding tissues or of blood, for example blood in arterial vessel. But note again, that is not "alway" the case.